Draft version September 18, 2020
Typeset using LaTeX **twocolumn** style in AASTeX63

Galaxian Contamination in Galactic Reddening Maps

Peter J. Brown [1,2] and Tate Walker[3]

[1] *Department of Physics and Astronomy, Texas A&M University, 4242 TAMU, College Station, TX 77843, USA*
[2] *George P. and Cynthia Woods Mitchell Institute for Fundamental Physics & Astronomy*
[3] *Department of Aerospace Engineering, Texas A&M University, 4242 TAMU, College Station, TX 77843, USA*

ABSTRACT

Estimating the amount of foreground extinction due to the Milky Way dust along the line of sight is often a first step in determining the luminosity of an object. The amount of Galactic dust inferred by infrared emission maps can be contaminated by infrared light from nearby galaxies. By comparing extinction values at and around the location of nearby galaxies, we compile a list of 92 galaxies which likely contaminate the maps with an excess of galaxian infrared emission and tabulate our recommend values for the MW contribution. A few cases where the infrared emission has been oversubtracted are also noted.

Keywords: dust: general, Milky Way: dust

1. INTRODUCTION

As luminosity is a fundamental property of astrophysical objects, properly correcting for the extinction of light due to dust is important. Accurate luminosities are needed for calculating energy budgets, sizes of objects, and the calibration and use of astrophysical objects as standard candles to measure distances in the universe.

Dust extinction can occur anywhere along the line of sight from an object to the observer, including circumstellar dust, dust in the host galaxy of an object, circumgalactic dust, intergalactic dust, and dust in our own Milky Way galaxy. These multiple components can make a full determination of the extinction complicated, but it is usually assumed that the component of dust extinction arising from the MW is the best understood. The all-sky dust reddening maps of Schlegel et al. (1998), hereafter referred to as SFD98, calibrated the luminosity at 100 μm from the Diffuse Infrared Background Experiment on the Cosmic Background Explorer (COBE/DIRBE) and the Infrared Astronomical Satellite (IRAS) and converted it into the V-band extinction using the colors of elliptical galaxies. These maps have made it convenient to look up the SFD98 reddening (or the rescaling by Schlafly & Finkbeiner 2011) via the NASA Extragalactic Database (NED[1]; Mazzarella et al. 2001) or other electronic queries without having to understand the data, read the paper, or notice the warnings from NED[2]. Combined with the mean value of R_V=3.1 from Fitzpatrick (1999) and ignoring the variations in the Milky Way (Clayton & Cardelli 1988) one has the extinction as a function of wavelength or can also implicitly assume those as well as the elliptical galaxy spectrum used by SFD98 and have the extinction readily computed in a number of common passbands. Such ease, however, often makes it too easy to overlook the details and complications extant in the data set.

Dalcanton et al. (2009) mentioned in a footnote that the SFD98 maps were contaminated by M82, brought to our knowledge through studies of the extinction toward the supernova (SN) 2014J (Foley et al. 2014). Johnson et al. (2009) cautioned about not just the contamination of M81 and M82 but also the highly variable region nearby. Chiang & Ménard (2019) found that galaxy clusters leave a small imprint on the dust maps. As dust reddening from anywhere has strong consequences in the ultraviolet, the authors were led to ask the question "Which nearby galaxies might be contaminating the dust maps in this same way?"

Corresponding author: Peter J. Brown
pbrown@physics.tamu.edu

[1] https://ned.ipac.caltech.edu/
[2] https://ned.ipac.caltech.edu/classic/help/faq3.html#3a

In this short paper we describe how we searched for examples of contaminating galaxies and give a table of recommended extinction values for the ones we found.

2. ANALYSIS

To detect likely point sources from galaxy contaminants in the dust maps, we searched for excesses in A_V at the center of each galaxy of interest compared to that $20'$ away in each of the four cardinal directions. We could then individually examine sources which were significantly higher than the mean of the $20'$ radius. As a baseline for what a significant excess is, we first looked up the A_V values (via IrsaDust.get_extinction_table in the Astroquery Python package) for 102 random positions in the sky. The central and mean radial values are plotted in Figure 1. As expected, most of the points cluster around the 1:1 line compared to the mean value in the surrounding points, and the scatter is a consistent fraction of the central value (note that both axis are on a log scale). From the random positions, we set one and two sigma limits of 12 % and 22% which encompass 68% and 95% of the points, respectively. A few points lie significantly below the 1:1 line due to bright spots in the angular regions.

We queried the A_V values at the location of each of the extragalactic sources in Rice et al. (1988), the 70 brightest of which should already have been removed from the SFD98 maps. For our scientific purposes, we also tabulated the nearby host galaxies used to calibrate the Cepheid-Supernova Ia distance ladder (Riess et al. 2016), the SINGS sample (Kennicutt et al. 2003), and over 700 supernova host galaxies observed by Swift (Brown et al. 2014). We manually examine the fields of all galaxies for which the central position has an A_V of 12% greater than the mean of the points at $20'$.

For each galaxy above our excess threshold, a square InfraRed Space ATLAS image (based on IRAS imaging) 100 μmimage $80'$across was created as well as a plot with the A_V as a function of radius out to $20'$ in each of the cardinal directions in steps of $1'$. Examples are shown in Figure 2. Both of these were visually examined to assess if the central excess was likely due to the flux of the galaxy, part of a region with highly variable infrared flux from the MW, or both. If the galaxy seemed to contribute to the excess, a value was chosen representing our best estimate of the A_V at the galaxy location and a radius within which that value should be used. For an isolated source, this corresponds to the background level. For galaxies in a region with a highly-variable foreground MW IR emission, such as a gradient, patchy emission, or artifacts, this was more subjective and used the IRAS image as a guide. Though imperfect, we believe our values to more accurately reflect the true MW reddening than the look up tables.

Some sources appear to be partially removed, replacing the pixels with the median value of a nearby annulus. The replaced region, however, is in some cases too small and the replacement value too bright in the regions passing our cuts. M51 and M83, as shown in Figure 2, are two examples of this. Visual examination of the Rice et al. (1988) galaxies was done to find galaxies with poor subtraction which nevertheless did not meet our criteria of having a significant central excess. M33 is a striking example which appears to be oversubtracted, as shown in 3. In some instances, such as NGC2442 and NGC4666, our recommended value is close to the replacement value used in the maps. The complexity of the location, however, leads to a higher recommended uncertainty, because the galaxy line of sight may or may not pass through the brighter regions of the foreground emission. In many cases our recommended value is not significantly different from the map value ($\sim$0.01 mag), but its use may avoid a small bias. Including a higher uncertainty recognizes that our knowledge of the MW dust is not as complete as is often assumed.

Other values returned from the tools are not properly corrected for the suggested corrections for the nearby Large and Small Magellanic clouds and M31 given in Appendix C of SFD98. The recommended value for the region around M31, for example, is E(B-V)=0.062. This is the value obtained from the NASA Extragalactic Database[3] when searching the position of M31. Since M31 is not removed from the maps, however, one obtains a value of E(B-V)=0.69 from the NASA/IPAC Infrared Science Archive from the website[4] or Astroquery in python.

Another problematic field we found was in the region of NGC4258. NGC4258 is an important rung of the extragalactic distance scale because of its geometrically-determined distance which is used either as a calibration of or a check of Cepheid distances (Macri et al. 2006; Humphreys et al. 2013; Hoffmann et al. 2016; Reid et al. 2019)[5]. There is a clear point source visible in some of the IRAS images. In most of the images available from the NASA/Infrared Processing and Analysis Center (IPAC), however, NGC4258 falls in a gap between data. This results in a discontinuity in the combined

[3] https://ned.ipac.caltech.edu/

[4] https://irsa.ipac.caltech.edu/frontpage/

[5] Fausnaugh et al. (2015) found an unusually grey extinction law for the Cepheids in NGC4258. It is beyond the scope of this paper to evaluate whether an incorrect value of the line of sight MW extinction could have a significant effect.

images. NGC88 also falls in a gap. These two cases are shown in the bottom panel of Figure 3.

Reading the mask values from the SFD data product would catch some of the source in or near the SMC, LMC, or M31 or for which no IRAS data existed and the DIRBE maps were used instead. These could be treated as a bug and corrected. Since past work may have been incorrectly analyzed, we are publishing this research article as well as notifying the developers in order to promote the best science in past and future analyses.

The values for the LMC, SMC and M31 recommended by Appendix C of SFD98 are corrected to the Schlafly & Finkbeiner (2011) system and listed in Table 1 along with the recommended value for M82 from Dalcanton et al. (2009). Thus one could query this table by position in order to update MW reddening values obtained from the IR maps. We note, however, that work requiring precise line of sight extinctions through these large areas should utilize other methods to better constrain the minimum position-dependent line of sight extinction contributed by the Milky Way in these extended areas (e.g. Haschke et al. 2011).

For those needing more precise values, improvements could be made by utilizing higher resolution images and a 2-dimensional modeling of the region around the galaxy. We have done our best to estimate an uncertainty based on the differences of the A_V values in the different directions and our visual inferences of what would be at the galaxy location. The list of contaminating galaxies is given in Table 1 with their central coordinates, the radius of contamination, our estimate for A_V, and our estimated uncertainty on A_V.

Many corrections for extinction already utilize the intrinsic colors of objects (e.g. type Ia supernovae; Phillips et al. 1999) to determine the total reddening to an object. An incorrect measure of the MW reddening could be compensated by a larger or smaller value of the host galaxy reddening. However this could be imprecise for the limiting cases of negligible host reddening and/or correcting for different reddening laws between the host galaxy and the MW dust.

3. SUMMARY

In summary, we have searched for galaxies whose infrared emission might significantly contaminate the IRAS images resulting in a overestimate of the foreground MW dust reddening. We provide a table of such galaxies, their coordinates, our recommended values on the Schlafly & Finkbeiner (2011) system, and the radius with which to use replacement values from those looked up by default from the SFD98 maps via NED or Astro-

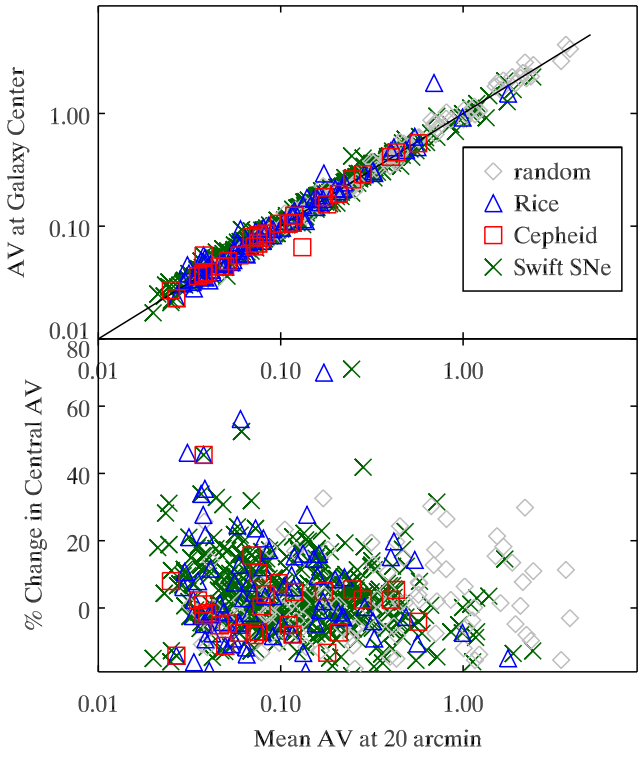

Figure 1: Top panel: The central value of A_V is plotted with respect to the mean of the A_V values 20′ away in each of the four cardinal directions. 102 random positions are plotted in grey. The sample from Rice et al. (1988) which should have already been removed are blue triangles. Nearby galaxies used to calibrate the Cepheid-SN distance ladder (Riess et al. 2016) are plotted as red squares. The sample of Swift supernovae are green crosses. A 1:1 line shows perfect agreement between the values. Bottom panel: A_V differences normalized by the mean A_V at 20′. The fractional difference is fairly constant with A_V. The fractional differences for the random locations have a standard deviation of 12%. This is used as the cutoff for our manual examination.

query. This will be communicated to the developers of such tools, and we make available our code to query our table or the dust maps as appropriate[6]. We recommend, however, that users make themselves aware of the issues of the data they use by reading the original papers even when the data products are made easily accessible via automated sources.

[6] https://github.com/pbrown801/AV

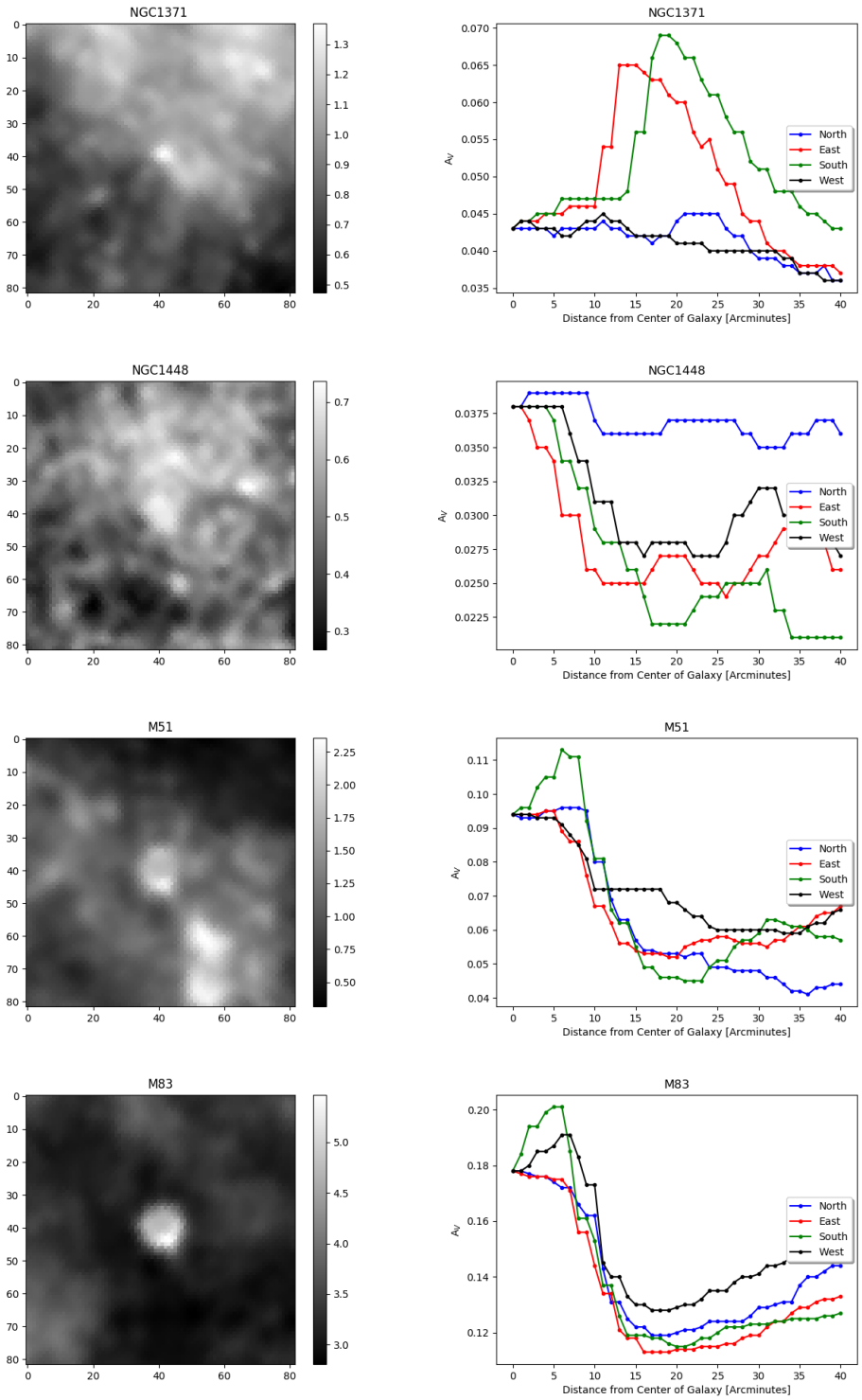

Figure 2: 100 μmIRAS images ($80' \times 80'$) on the left and the corresponding plots of A_V v. distance from center for a few galaxies illustrating the range of contamination. The top panel shows the small but clear contribution of NGC1371. The second panel shows the more complicated field of NGC1448. The bottom two panels show the uncomplete subtraction of M51 and M83.

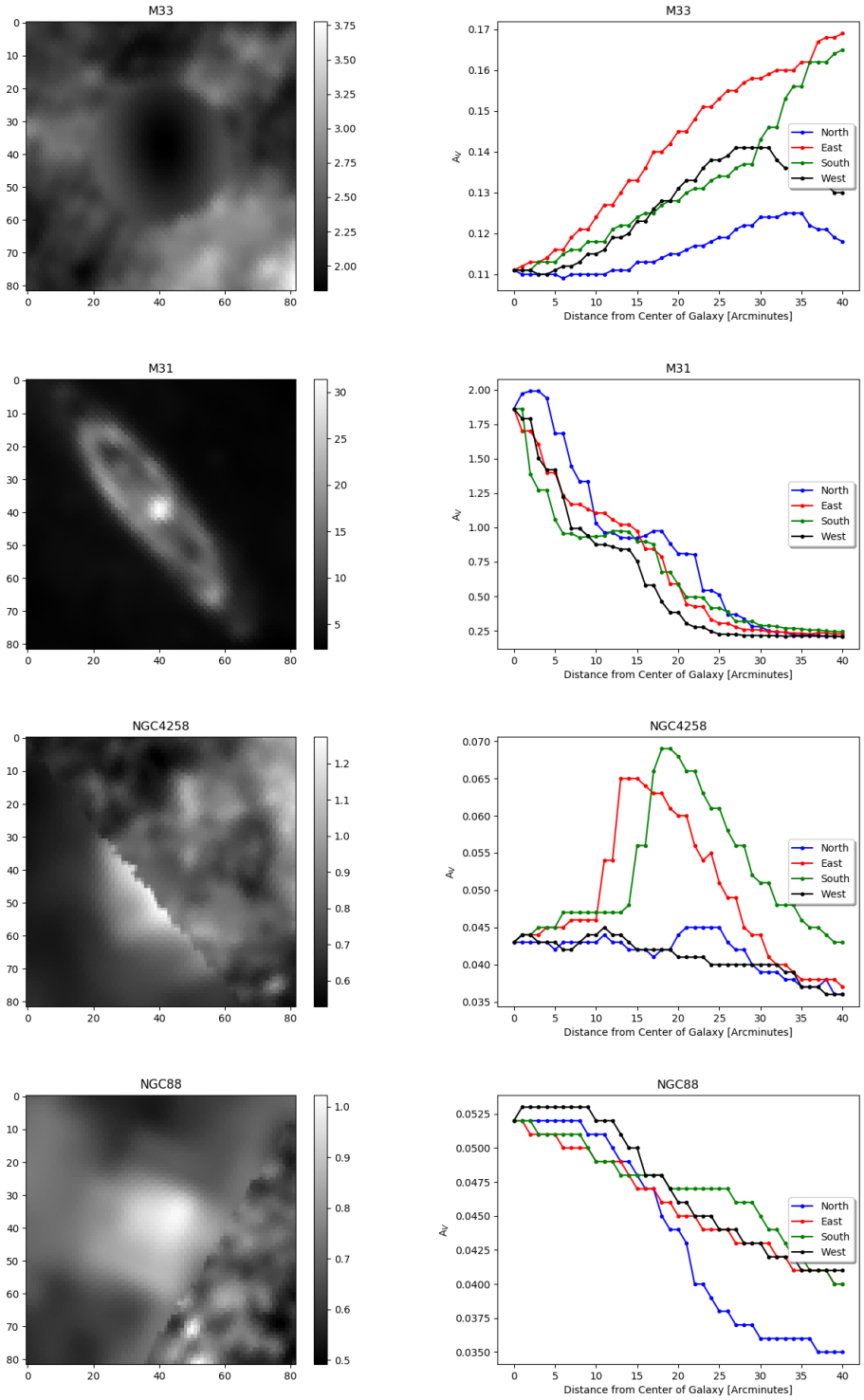

Figure 3: 100 μmIRAS images ($80' \times 80'$) on the left and the corresponding plots of A_V v. distance from center for a few galaxies illustrating the range of contamination. In the first row, M33 has been oversubtracted, so the MW reddening would be underestimated. In the second panel, M31 has not been removed, with the recommended value from the appendix of SFD98 being reported by NED but not IRSA. The bottom panels show discontinuities in the reddening values near NGC4258 and NGC88 due to data gaps in the IRAS imaging.

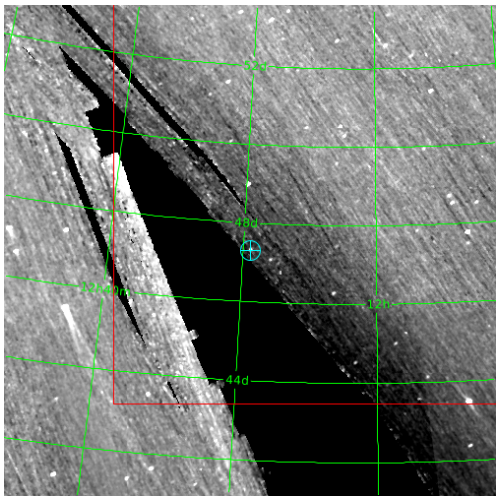

Figure 4: 100 μm A wider-field IRAS image (12.5 degrees across) of NGC4258 showing the gaps in the IRAS imaging.

ACKNOWLEDGMENTS

Most of this work was done as a student project as part of Texas A&M's Aggie Research Program.

Software: astropy (Astropy Collaboration et al. 2013; Price-Whelan et al. 2018), scipy (Jones et al. 2001–; Virtanen et al. 2019)

REFERENCES

Astropy Collaboration, Robitaille, T. P., Tollerud, E. J., et al. 2013, A&A, 558, A33, doi: 10.1051/0004-6361/201322068

Brown, P. J., Breeveld, A. A., Holland, S., Kuin, P., & Pritchard, T. 2014, A&SS, 354, 89, doi: 10.1007/s10509-014-2059-8

Chiang, Y.-K., & Ménard, B. 2019, ApJ, 870, 120, doi: 10.3847/1538-4357/aaf4f6

Clayton, G. C., & Cardelli, J. A. 1988, AJ, 96, 695, doi: 10.1086/114838

Dalcanton, J. J., Williams, B. F., Seth, A. C., et al. 2009, ApJS, 183, 67, doi: 10.1088/0067-0049/183/1/67

Fausnaugh, M. M., Kochanek, C. S., Gerke, J. R., et al. 2015, MNRAS, 450, 3597, doi: 10.1093/mnras/stv881

Fitzpatrick, E. L. 1999, PASP, 111, 63, doi: 10.1086/316293

Foley, R. J., Fox, O. D., McCully, C., et al. 2014, MNRAS, 443, 2887, doi: 10.1093/mnras/stu1378

Haschke, R., Grebel, E. K., & Duffau, S. 2011, AJ, 141, 158, doi: 10.1088/0004-6256/141/5/158

Hoffmann, S. L., Macri, L. M., Riess, A. G., et al. 2016, ApJ, 830, 10, doi: 10.3847/0004-637X/830/1/10

Humphreys, E. M. L., Reid, M. J., Moran, J. M., Greenhill, L. J., & Argon, A. L. 2013, ApJ, 775, 13, doi: 10.1088/0004-637X/775/1/13

Johnson, L. C., Méndez, R. H., & Teodorescu, A. M. 2009, ApJ, 697, 1138, doi: 10.1088/0004-637X/697/2/1138

Jones, E., Oliphant, T., Peterson, P., et al. 2001–, SciPy: Open source scientific tools for Python. http://www.scipy.org/

Kennicutt, Robert C., J., Armus, L., Bendo, G., et al. 2003, PASP, 115, 928, doi: 10.1086/376941

Macri, L. M., Stanek, K. Z., Bersier, D., Greenhill, L. J., & Reid, M. J. 2006, ApJ, 652, 1133, doi: 10.1086/508530

Mazzarella, J. M., Madore, B. F., & Helou, G. 2001, in Proc. SPIE, Vol. 4477, Astronomical Data Analysis, ed. J.-L. Starck & F. D. Murtagh, 20–34, doi: 10.1117/12.447177

Phillips, M. M., Lira, P., Suntzeff, N. B., et al. 1999, AJ, 118, 1766, doi: 10.1086/301032

Price-Whelan, A. M., Sipőcz, B. M., Günther, H. M., et al. 2018, AJ, 156, 123, doi: 10.3847/1538-3881/aabc4f

Reid, M. J., Pesce, D. W., & Riess, A. G. 2019, ApJL, 886, L27, doi: 10.3847/2041-8213/ab552d

Rice, W., Lonsdale, C. J., Soifer, B. T., et al. 1988, ApJS, 68, 91, doi: 10.1086/191283

Riess, A. G., Macri, L. M., Hoffmann, S. L., et al. 2016, ApJ, 826, 56, doi: 10.3847/0004-637X/826/1/56

Schlafly, E. F., & Finkbeiner, D. P. 2011, ApJ, 737, 103, doi: 10.1088/0004-637X/737/2/103

Schlegel, D. J., Finkbeiner, D. P., & Davis, M. 1998, ApJ, 500, 525, doi: 10.1086/305772

Virtanen, P., Gommers, R., Oliphant, T. E., et al. 2019, arXiv e-prints, arXiv:1907.10121. https://arxiv.org/abs/1907.10121

Table 1. Improved Estimates for the Galactic Extinction in the Line of Sight near External Galaxies in the Schlafly & Finkbeiner (2011) System

Galaxy Name	RA (H M S)	Dec (D M S)	Radius (arcmin)	Map A_V (mag)	A_V (mag)	Err(a) (mag)	Supernovae
LMC	05h23m34.6s	-69d45m22s	323	2.419	0.20(b)	0.05	SN1987A
SMC	00h52m38.0s	-72d48m01s	190	1.188	0.10(b)	0.05	...
M31	00h42m44.5s	+41d16m09s	95	1.862	0.17(b)	0.05	SN1885A
M82	9h55m52.43s	69d40m46.93s	20	0.419	0.16(c)	0.05	SN2004am, SN2008iz, SN2014J, SN2019ajl
Arp244	12h01m53.17s	-18d52m37.92s	15	0.124	0.11	0.01	SNe 1921A, 1974E, 2004gt, 2007sr, 2013dk
ESO138-G10	16h59m02.952s	-60d12m57.67s	12	0.591	0.55	0.05	SN2013by
ESO287-G40	21h37m28.1842s	-47d02m08.8331s	7	0.077	0.065	0.01	SNe 2009lc, 2013fy
ESO317-32	10h28m01.6186s	-42d06m38.7541s	12	0.363	0.33	0.03	SN2017ghs
ESO509-IG064	13h34m39.3s	-23d40m50s	15	0.339	0.3	0.02	SN2016eiy
IC208	2h08m27.736s	6d23m41.53s	12	0.147	0.13	0.01	SNe 2003G, 2017glq
IC2574	10h28m23.6205s	68d24m43.4414s	15	0.097	0.08	0.01	...
IC5249	22h47m06.262s	-64d49m55.42s	15	0.092	0.08	0.01	SN2011cb
KUG0647+311	6h50m36.832s	31d07m00.6s	15	0.356	0.31	0.03	SN2016asf
M51	13h29m52.698s	47d11m42.93s	15	0.094	0.05	0.01	SNe 1945A, 1994I, 2005cs, 2011dh
M61	12h21m54.9275s	4d28m25.5883s	15	0.06	0.05	0.01	SNe 1926A, 1964F, 1961I, 1999gn
M61	...	...	...	...	...	...	SNe 2006ov, 2008in, 2014dt
M66	11h20m15.026s	12d59m28.64s	15	0.09	0.07	0.01	SN1973R, SN1989B, SN1997bs
M66							SN2009hd, SN2016cok
M74	1h36m41.772s	15d47m00.46s	15	0.188	0.16	0.02	SNe 2002ap, 2003gd, 2013ej, PS15blm
M83	13h37m00.919s	-29d51m56.74s	15	0.178	0.12	0.01	SNe 1923A, 1945B, 1950B
M83							SNe 1957D, 1968L, 1983N
MCG-01-07-004	2h23m13.2516s	-4d31m01.5168s	7	0.08	0.07	0.05	SNe ASASSN-15od, SCP06R12, PS1-10g
MCG-02-24-027	9h28m59.256s	-14d48m27.25s	7	0.188	0.17	0.01	SN2011at
MCG-02-30-003	11h33m10.5799s	-10d13m43.7361s	10	0.113	0.09	0.01	SNe 2003ee, 2017hm
MCG+10-19-1	12h54m49.706s	58d52m56.46s	7	0.032	0.025	0.005	PTF10icb
NGC0584	1h31m20.755s	-6d52m05.02s	15	0.114	0.1	0.01	SN2016fng

Table 1 *continued*

Table 1 *(continued)*

Galaxy Name	RA (H M S)	Dec (D M S)	Radius (arcmin)	Map A_V (mag)	A_V (mag)	Err(a) (mag)	Supernovae (mag)
NGC1097	2h46m19.059s	-30d16m29.68s	15	0.072	0.05	0.01	SNe 1992bd, 1999eu, 2003B
NGC1313	3h18m16.046s	-66d29m53.74s	20	0.293	0.1	0.05	SNe 1962M, 1978K
NGC134	0h30m21.893s	-33d14m43.26s	20	0.049	0.03	0.01	SN2009gj
NGC1365	3h33m36.458s	-36d08m26.37s	20	0.055	0.03	0.01	SNe 1957C, 1983V, 2001du, 2012fr
NGC1371	3h35m01.351s	-24d55m59.19s	10	0.072	0.05	0.01	SN2005ke
NGC1448	3h44m31.915s	-44d38m41.38s	10	0.038	0.025	0.01	SNe 1983S, 2001el, 2003hn, 2014df
NGC2315	7h02m33.038s	50d35m26.18s	7	0.226	0.2	0.02	SN2011ay
NGC2357	7h17m40.981s	23d21m24.28s	10	0.178	0.15	0.02	SN2010bj, SN2015I
NGC2442	7h36m23.84s	-69d31m51.0s	7	0.556	0.55	0.05	SN1999ga, SN2015F
NGC253	00h47m33.120s	-25d17m17.59s	20	0.051	0.045	0.005	SN1940E
NGC2577	8h22m43.45s	22d33m11.1408s	10	0.145	0.12	0.01	SN2007ax
NGC2615	8h34m33.358s	-2d32m48.57s	10	0.096	0.075	0.005	SN2014ao
NGC2668	8h49m22.57s	36d42m37.53s	10	0.095	0.085	0.005	SN2003je
NGC2748	9h13m43.037s	76d28m31.23s	5	0.071	0.06	0.01	SN1985A, SN2013ff, PS15jf, 2017gkk
NGC2811	9h16m11.1s	-16d18m45.78s	12	0.145	0.12	0.01	SN2005am, SN2018jzo
NGC3521	11h05m48.5676s	-0d02m09.2282s	15	0.154	0.11	0.02	...
NGC3556	11h11m30.967s	55d40m26.84s	20	0.045	0.025	0.005	SN1969B
NGC3690	11h28m31.326s	58d33m41.8s	10	0.045	0.035	0.01	SN1992bu, SN1993G, SN1998T
NGC3690							SN2010O, SN2010P, SN2019lqo
NGC3690							SN2010O, SN2010P, SN2019lqo
NGC383	1h07m24.9587s	32d24m45.214s	14	0.193	0.16	0.02	SNe 2000dk, 2015ar, 2016sx, 2017hle
NGC3953	11h53m49.0088s	52d19m36.4738s	15	0.08	0.06	0.01	SNe 2001dp, 2006bp
NGC4080	12h04m51.804s	26d59m33.43s	12	0.068	0.055	0.005	MASTER OT J120451.50+265946.6
NGC4214	12h15m39.174s	36d19m36.8s	10	0.059	0.06	0.005	SNe 1954A, 2010U
NGC4569	12h36m49.816s	13d09m46.33s	7	0.126	0.12	0.01	...
NGC4594	12h39m59.4319s	-11d37m22.9954s	10	0.137	0.135	0.005	SNe 1997bl, PS15akv
NGC4631	12h42m08.009s	32d32m29.44s	10	0.046	0.045	0.005	...
NGC4736	12h50m53.148s	41d07m12.55s	15	0.048	0.035	0.01	...
NGC5055	13h15m49.2739s	42d01m45.7261s	15	0.047	0.035	0.01	SN1971I

Table 1 *continued*

Table 1 *(continued)*

Galaxy Name	RA (H M S)	Dec (D M S)	Radius (arcmin)	Map A_V (mag)	A_V (mag)	Err(a) (mag)	Supernovae
NGC5177	13h29m24.269s	11d47m49.55s	5	0.093	0.08	0.01	SN2010cr
NGC5221	13h34m55.909s	13d49m57.14s	10	0.079	0.065	0.01	SN1970P, SN2008ez, PS1-14ea, SN2016bln
NGC5490	14h09m57.33s	17d32m43.53s	10	0.073	0.065	0.005	SN1997cn, SN2003aq
NGC5490							SN2005I, SN2015bo, SN2016ccm
NGC613	1h34m18.235s	-29d25m06.56s	15	0.052	0.045	0.005	SN2016gkg
NGC6166	16h28m38.2444s	39d33m04.2318s	10	0.03	0.025	0.005	SN1997cq, SN2009eu
NGC6166							PS15aot, SN2018ccl, SN2019gqd
NGC634	1h38m18.679s	35d21m53.47s	10	0.145	0.12	0.01	SN2006Q, SN2008A
NGC6479	17h48m21.5875s	54d08m56.4765s	7	0.115	0.095	0.01	SN2007cl, SN2009ay
NGC6822	19h44m56.199s	-14d47m51.29s	20	0.621	0.55	0.05	···
NGC7187	22h02m44.4954s	-32d48m11.439s	10	0.092	0.08	0.01	SN2017gah
NGC7259	22h23m05.5451s	-28d57m17.4766s	7	0.055	0.045	0.005	SN2009ip, SN2014dq, SMT16jyu
NGC7371	22h46m03.744s	-11d00m04.3327s	7	0.165	0.15	0.005	LSQ13cux, PS15bgt
NGC7552	23h16m10.767s	-42d35m05.39s	12	0.038	0.03	0.005	SN2017bzc
NGC7653	23h24m49.3612s	15d16m32.1419s	7	0.179	0.18	0.02	SN2015bf, SN2018cjk
NGC7793	23h57m49.7534s	-32d35m27.7083s	12	0.052	0.035	0.01	SN2008bk
NGC88	0h21m22.132s	-48d38m24.28s	20	0.052	0.04	0.01	SN1994Z, ASASSN-15ut
NGC918	2h25m50.7911s	18d29m46.3842s	20	0.945	0.7	0.1	SN2009js, SN2011ek
PGC071943	23h37m44.414s	-47d30m22.92s	10	0.043	0.03	0.005	···
PGC2692384	18h32m24.016s	66d53m43s	15	0.206	0.16	0.02	SN2011hj
PGC29010	10h01m26.5223s	36d40m16.6648s	8	0.041	0.03	0.005	SN2012ak, PS15ahw
PGC68345	22h14m03.018s	-26d56m15.77s	10	0.075	0.06	0.005	SN2010bv, SN2016dgt
PGC83768	13h02m35.193s	27d26m21.38s	12	0.029	0.025	0.005	SN1962I, SN1991Q, SN2003do, SN2012da
PGC9204	2h25m28.346s	-25d38m16.46s	10	0.045	0.035	0.005	SN2014cp
SDSSJ161609.48+383245.0	16h16m09.485s	38d32m45.09s	7	0.043	0.03	0.005	SN2013eh
UGC09113	14h14m14.762s	35d25m23.83s	15	0.063	0.045	0.005	···
UGC09386	14h34m52.7783s	40d44m52.8518s	15	0.042	0.035	0.005	SN2017daf
UGC10064	15h51m13.2752s	25d42m06.784s	13	0.187	0.16	0.01	SN2009dc, SN2019fee
UGC10214	16h06m03.94s	55d25m31.33s	5	0.025	0.02	0.005	SN2002lk, SN2007cu, SN2008dq

Table 1 *continued*

Table 1 *(continued)*

Galaxy Name	RA (H M S)	Dec (D M S)	Radius (arcmin)	Map A_V (mag)	A_V (mag)	Err(a) (mag)	Supernovae
UGC10214							PS1-10acx, PS1-11agk
UGC10685	17h04m50.999s	12d55m29.64s	10	0.269	0.24	0.02	SN2010hw, SN2013cj
UGC11501	19h58m37.031s	2d36m10.62s	10	0.462	0.37	0.05	SN2011dn
UGC11797	21h43m20.1605s	43d34m34.644s	10	1.434	1.25	0.1	SN2004ca, SN2015N, SN2018dfy
UGC12640	23h30m56.799s	15d29m25.96s	10	0.184	0.17	0.01	SN2011ef, SN2019ssi
UGC12846	23h55m46.0248s	18d25m33.6036s	10	0.1	0.09	0.01	SN2007od
UGC12850	23h56m06.16s	29d22m40.44s	10	0.17	0.14	0.015	SN2014ek, CSSJ235535.6+291220
UGC2855	3h48m20.731s	70d07m58.37s	7	1.943	1.9	0.2	SN2014dg
UGC402	0h39m18.612s	3d57m08.87s	10	0.069	0.065	0.005	ASASSN-15qc, SN2016hsq
UGC4179	8h02m05.9609s	0d48m32.742s	5	0.153	0.14	0.02	SN2006jd
UGC5055	9h30m11.7493s	55d51m08.6863s	8	0.091	0.07	0.02	SN2014R
UGC5378	10h00m31.9918s	4d24m25.6711s	5	0.075	0.065	0.005	SN2007S
UGC5460	10h08m09.197s	51d50m40.2504s	5	0.029	0.02	0.005	SN2011ht, SN2015as
UGC5623	10h23m48.6038s	33d48m28.7892s	9	0.065	0.055	0.005	SN2010ks
UGC6483	11h29m02.358s	17d13m55.15s	7	0.082	0.065	0.005	SN2013hh
UGC7848	12h40m57.433s	63d31m11.3s	5	0.041	0.035	0.005	SN2006bv
UGC8713	13h47m01.2595s	33d53m36.9528s	10	0.057	0.05	0.005	SN2012cp

[a] This is the uncertainty on what the extinction would be from the Schlegel et al. (1998) maps converted to the Schlafly & Finkbeiner (2011) system. It does not include the overall 16% uncertainty of the maps themselves quoted by Schlegel et al. (1998) which should be added in quadrature.

[b] Value from Appendix C of Schlegel et al. (1998) converted to the Schlafly & Finkbeiner (2011) system.

[c] Value from Dalcanton et al. (2009) converted to the Schlafly & Finkbeiner (2011) system.